Hindawi Publishing Corporation
International Journal of Photoenergy
Volume 2013, Article ID 768348, 9 pages
http://dx.doi.org/10.1155/2013/768348

Research Article

Influence of Ce Doping on the Electrical and Optical Properties of TiO_2 and Its Photocatalytic Activity for the Degradation of Remazol Brilliant Blue R

Aisha Malik,[1] S. Hameed,[1] M. J. Siddiqui,[2] M. M. Haque,[3] and M. Muneer[3]

[1] *Department of Electrical Engineering, Aligarh Muslim University, Aligarh 202002, India*
[2] *Department of Electronics Engineering, Aligarh Muslim University, Aligarh 202002, India*
[3] *Department of Chemistry, Aligarh Muslim University, Aligarh 202002, India*

Correspondence should be addressed to Aisha Malik; aishasamra@gmail.com

Received 31 May 2013; Revised 16 September 2013; Accepted 18 September 2013

Academic Editor: Jimmy Yu

Nanocrystalline TiO_2 particles doped with different concentrations of Cerium (Ce, 1–10%) have been synthesized using sol-gel method. The prepared particles were characterized by standard analytical techniques such as X-ray diffraction (XRD), FTIR and Scanning Electron Microscopy (SEM), and Transmission Electron Microscopy (TEM). The XRD analysis shows no change in crystal structure of TiO_2 after doping with different concentrations of Ce, which indicates the single-phase polycrystalline material. The SEM analysis shows the partial crystalline nature of undoped, and doped TiO_2 and TEM analysis shows the particle sizes were in the range of 9–14 nm in size. The a.c. analysis shows that the dielectric constant ε and dielectric loss tan δ decrease with the increase in frequency. The dielectric property decreases with the increase in dopant concentration. It is also observed that the impedance increases with an increase in dopant concentration. The photocatalytic activity of the synthesized particles (Ce-doped TiO_2) with dopant concentration of 9% (Ce) showed the highest photocatalytic activity for the degradation of the dye derivative Remazol Brilliant Blue R in an immersion well photochemical reactor with 500 W halogen linear lamp in the presence of atmospheric oxygen.

1. Introduction

Due to the large surface area for the interaction of visible light, the synthesis of nanostructured semiconductor particles attracted greater attention during last few years [1]. TiO_2, a semiconductor has received the greater attention due to nontoxic, easily available, resistant to photocorrosion, and high catalytic efficiency [2, 3]. Due to the large band gap of TiO_2 (3.2 eV), the material limits the use of visible light. This property inhibits the use of solar spectrum as a light source. To enhance the catalytic property of TiO_2 under the visible light many attempts have been made to change the physical and chemical compositions of TiO_2 by doping with metals/nonmetals such as V, Cr, Mn, Fe, Ni, and Cu. In order to extend the optical absorption of the catalyst to the visible spectrum region many studies have been reported employing different methodologies [4–9]. The various methods used for doping of TiO_2 involve ion implantation, sol-gel reaction, hydrothermal reaction, solid-state reaction, and so forth [10–13]. Out of which the sol-gel process is undoubtedly the simplest and the cheapest one and also it provides control on the size and shape of nanoparticles. As it is well known that UV irradiation requires high energy source and is costlier and hazardous [14]. Hence, the use of visible light is preferred.

To characterize the electrical property impedance spectroscopy is an effective method. It can resolve the grain and grain boundary contribution to the system and calculate the conductivity and dielectric constant [15]. Recently much more attention has been given to the TiO_2 because of having stable dielectric properties which is characterized by high relative dielectric constant and low dielectric loss [16]. It is having an important application such as high density, dynamic memory device, microelectronics device, and microcommunication system [17–20].

The present paper deals with the synthesis of Ce-doped TiO_2 with different concentrations of metal ions using sol-gel method followed by characterization using standard

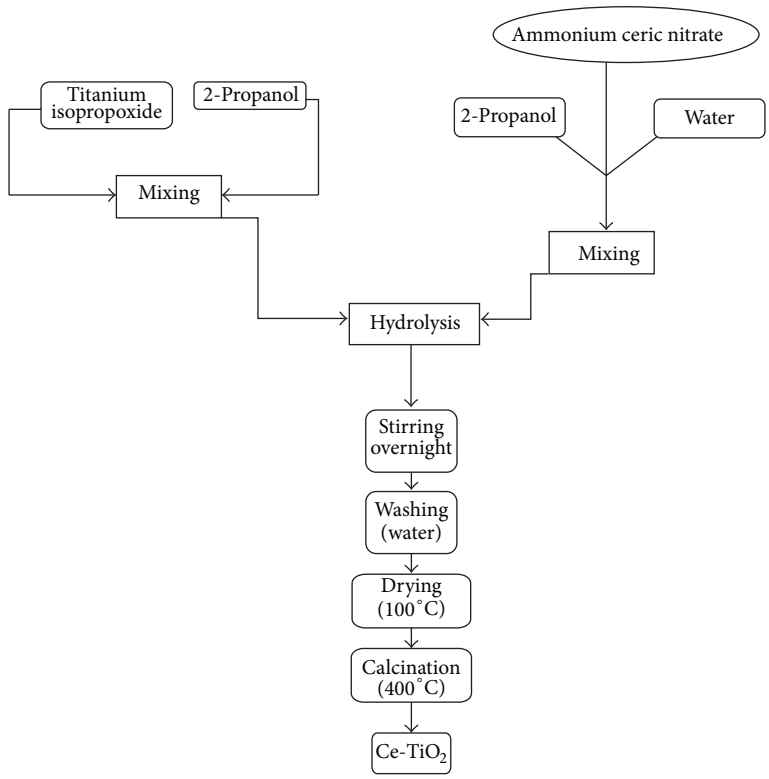

Figure 1: Typical procedure of Ce-TiO_2 preparation by sol-gel method.

analytical techniques such as X-ray diffraction (XRD), UV-Vis spectroscopy, Scanning Electron Microscopy (SEM), and Transmission Electron Microscopy (TEM). Also in this work, the computer control LCR meter analyser is used for Complex impedance spectroscopy for a wide range of frequencies. The impedance analysis gives the maximum possible information about the material [21]. The activity of the synthesized photocatalyst was also tested by studying the degradation of a textile dye derivative Remazol Brilliant Blue R under visible light source.

2. Experimental Details

2.1. Reagents and Chemicals. High purity Titanium isopropoxide and Remazol Brilliant Blue R were purchased from Sigam-Aldrich; Ammonium ceric nitrate, 2-propanol and ethanol were purchased from Rankem, CDH, and SD Fine-Chem. Ltd. India, respectively.

2.2. Apparatus. The structural characterization of undoped TiO_2 and doped TiO_2 nanoparticles was performed by XRD in the 2θ range of 20–80° (RigakuMiniflex II) with Cu Kα radiations (λ = 1.5418 Å) operated at voltage of 30 kV and-current of 15 mA. The UV-Vis spectra were recorded at room temperature in the range of 300–800 nm using Shimadzu UV-Vis spectrophotometer (Model 1601). The morphology and size were observed by SEM (Leo 435 VP) and TEM (Jeol 2100F). Electrical properties were measured using computer control LCR meter analyser (Model Agilant 48).

2.3. Preparation of TiO_2 and Ce-TiO_2. Undoped TiO_2 was prepared by sol-gel process with titanium isopropoxide as the titania precursor. For this, twenty five mL water was first dissolved in twenty five mL of 2-propanol. The second solution was prepared by dissolving 0.1 M titanium isopropoxide completely in 125 mL of 2-proponal. Both the solutions were sealed immediately and stirred rapidly using magnetic stirrer to obtain homogeneous solutions. The 2-propanol solutions containing water were then added dropwise to the alkoxide part under continuous stirring. This would result in the hydrolysis of titanium isopropoxide due to reaction with water by changing the colour of the solution from colourless to white. After the complete addition of the water part of the solution to that of the alkoxide part, the resulting solution was stirred overnight and then filtered under reduced pressure. For doping of TiO_2 particle with Ce, a known concentration of $(NH_4)_2Ce(NO_3)_6$ (1–10%, w/v) was added to the solution containing water and 2-propanol which was then added to titanium isopropoxide solution. The residue was washed with double distilled water and ethanol several times and then kept in oven at 100°C for complete removal of water and solvent. The dried residue was manually grinded in agate mortar and then calcined at 400°C for 4 h (Figure 1).

The synthesized nanoparticles were regrind and mixed with binder (polyvinyl alcohol), the mixture was then heated at 300°C to burn out the binder. Further a pellet of 13 mm in diameter and of thickness 1.8 mm were made by applying pressure up to 7 tonn/cm^2 on the powder sample by using hydraulic press. The pallet was then used for electrical

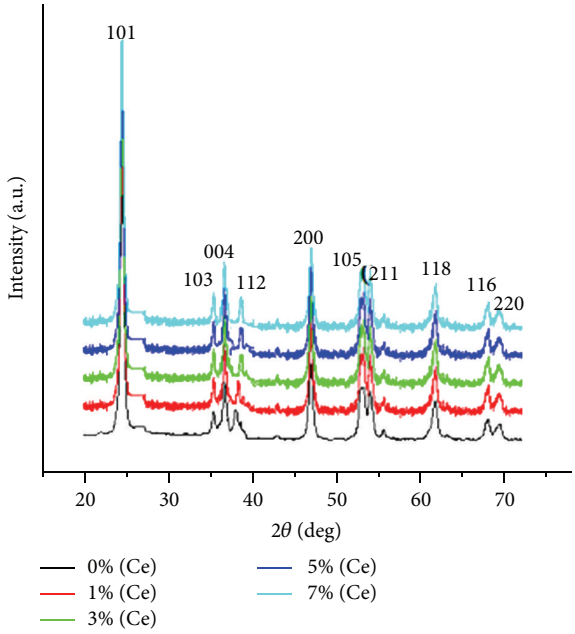

Figure 2: XRD patterns of undoped TiO_2 and Ce-TiO_2 with different concentrations of Ce. Calcination temp: 400°C and calcination time: 4 h.

measurement by coating the opposite faces with silver paste to form parallel plate capacitor.

2.4. Photocatalytic Experiments. The solutions of desired concentration of dye derivatives Remazol Brilliant Blue R (0.05 Mm) were prepared in double distilled water. An immersion well photochemical reactor made of Pyrex glass was used in this study. For irradiation experiments, an aqueous solution (200 mL) of dye was taken into the reactor and the required amount of photocatalyst (TiO_2/doped TiO_2, 1 gL^{-1}) was added and the solution was stirred and bubbled with atmospheric oxygen for at least 15 minutes in the dark to allow equilibration of the system so that the loss of dye due to adsorption can be taken into account. The zero time reading was obtained from a blank solution kept in the dark but otherwise treated similarly to the irradiated solution. Irradiations were carried out using a visible light halogen linear lamp (500 W, 9500 Lumens). Samples (10 mL) were collected before and at regular intervals during the irradiation and centrifuged before analysis.

3. Results and Discussion

3.1. Optical Properties

3.1.1. X-Ray Diffraction. The structural characterization of pure and Ce-doped TiO_2 nanoparticles was performed by X-ray diffraction (XRD) in the 2θ range of 20–80° (Rigaku Miniflex II) with Cu Kα radiations (λ = 1.5418 Å) operated at voltage of 30 kV and current of 15 mA. Figure 2 shows the crystal structure of undoped TiO_2 and Ce-doped TiO_2 as determined by X-ray diffraction. The diffraction patterns of doped powders were similar with those of pure anatase TiO_2.

Table 1: Crystallite size of Ce-doped TiO_2 with different concentration of Ce. Calcination temp: 400°C and calcination time: 4 h.

Sample number	Ce concentration (%)	Crystallite size (nm)
1	0	8.2
2	1.0	7.2
3	3.0	6.8
4	5.0	6.4
5	7.0	6.0

The average anatase crystallite size was determined by Scherer formula [22] as given by

$$D = \frac{K\lambda}{\beta \cos\theta}, \quad (1)$$

where D = crystallite size, K = shape factor, λ = wavelength, θ = diffraction angle, and β = full width at half maximum. The mean size of the crystallites in samples was estimated by the FWHM of the XRD peak (101) using the Debye-Scherer equation, as given in Table 1. The data obtained from the Scherer equation shows decrease in crystallite size with an increase in Ce content. This trend can be explained on the basis of the fact that the addition of dopant may hinder the growth of TiO_2 particle to some degree [23].

3.1.2. Scanning Electron Microscopy. The microstructural characterization of TiO_2 and Ce-doped TO_2 nanoparticles was carried out by Scanning Electron Microscopy. The morphology of undoped and 7% Ce-doped TiO_2 particles calcined at 400°C for 4 h are presented in Figures 3(a) and 3(b), respectively. The SEM images of undoped and doped TiO_2 at different magnifications show the partial crystalline nature. After doping the morphology of doped material remains unchanged, showing the amorphous nature with rough surfaces.

3.1.3. Transmission Electron Microscopy. The morphology of 7%-doped TiO_2 particles calcined at 400°C using Transmission Electron Microscopic technique (TEM) is shown in Figure 4. The TEM image of 7% Ce-doped TiO_2 shows that particles are spherical and fully crystallized. The particle size is found to be 9–14 nm.

3.1.4. FTIR Absorption Analysis. The FTIR spectra of Ce-doped TiO_2 (0–7%) powder calcined for 4 h at 400°C are presented in Figure 5. The presence of transmittance bands between 3400 and 3600 cm^{-1} are seen, which increased by doping Ce in TiO_2 while transmittance bands at 1625 cm^{-1} decreases with increase in doping Ce content in TiO_2. These bands are attributed to the stretching vibrations of the O–H groups and the bending vibrations of the adsorbed water molecules, respectively [24, 25]. A band between 650 and 830 cm^{-1} is seen which is attributed to different vibrational modes of TiO_2. Anatase phases of TiO_2 exhibit strong FT-IR absorption bands in the regions of 850–650 cm^{-1} [26, 27]. The band seen below 1200 cm^{-1} is due to Ti–O–Ti vibrations.

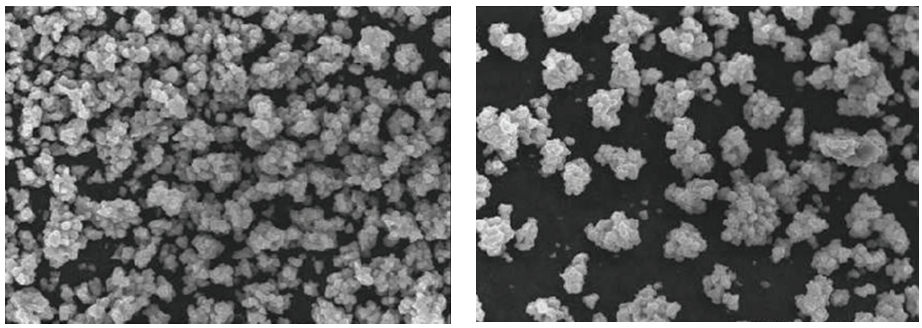

(a) Undoped TiO_2 Calcination temp: 400°C and calcination time: 4 h

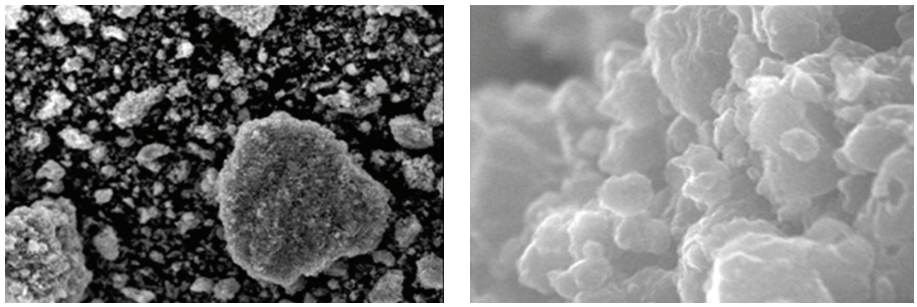

(b) 7% Ce-TiO_2 Calcination temp: 400°C, calcination time: 4 h

Figure 3: SEM micrographs of undoped TiO_2 and Ce-doped TiO_2.

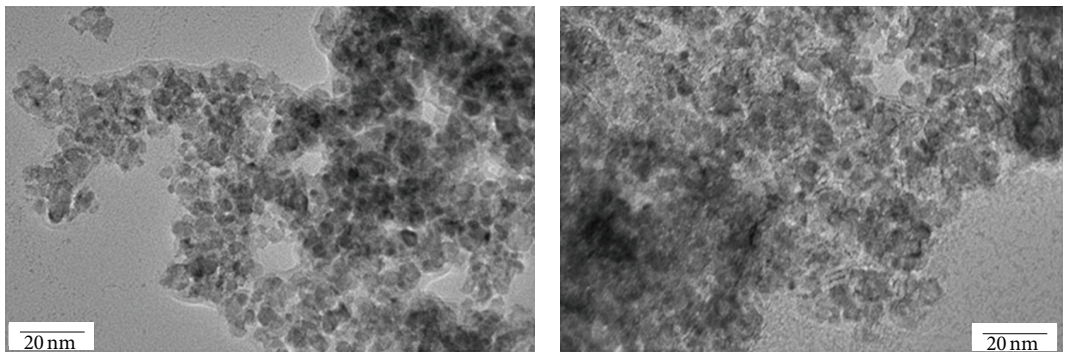

Figure 4: TEM micrographs of 7% Ce-TiO_2, Calcination temp: 400°C and calcination time: 4 h.

3.1.5. UV-Vis Absorption Spectra. The UV-Vis absorption spectra of undoped TiO_2 and Ce-doped TiO_2 with different dopant concentrations of Ce was studied and the results are shown in Figure 6. The band gap energies of undoped and Ce-doped TiO_2 particles with the obtained wavelength from UV-Vis absorption spectra were calculated using the following [28]

$$\text{Band gap (ev)} = \frac{1240}{\text{wavelength (nm)}}. \quad (2)$$

The band gap energies of undoped and Ce-doped TiO_2 with dopant concentrations (1–10%) are listed in Table 2. As expected, incorporation of dopant (Ce) into TiO_2 lattice has been found to shift the fundamental absorption edge towards the longer wavelength, that is, red shift, which decreases the band gap energy upto 9% dopant concentration [29, 30]. Further increase in dopant concentration (10%) leads to increase in band gap energy. This may be due to the deposition of the metal on the photocatalyst which covered the surface of TiO_2 and can reduce the effective surface area for absorbing light [31].

Table 2: Band gap energy of Ce-doped TiO_2 with different concentration of Ce. Calcination temp: 400°C and calcination time: 4 h.

S. no.	Ce concentration (%)	Band gap (eV)
1	0.0	3.07
2	1.0	3.04
3	3.0	3.01
4	5.0	2.87
5	7.0	2.72
6	8.0	2.70
7	9.0	2.66
8	10	2.69

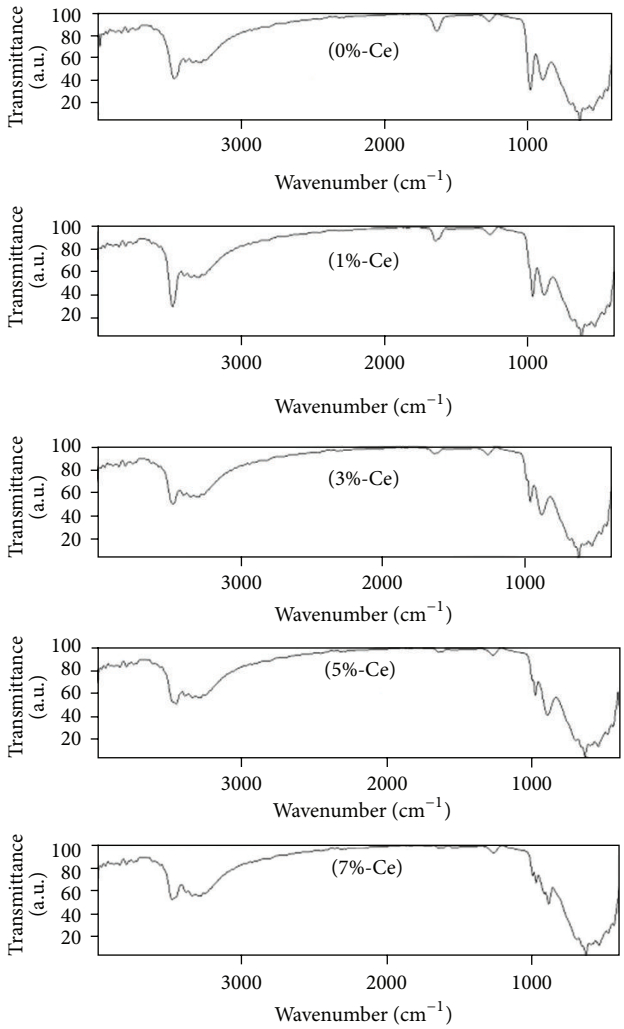

Figure 5: FTIR of undoped and Ce-doped TiO_2.

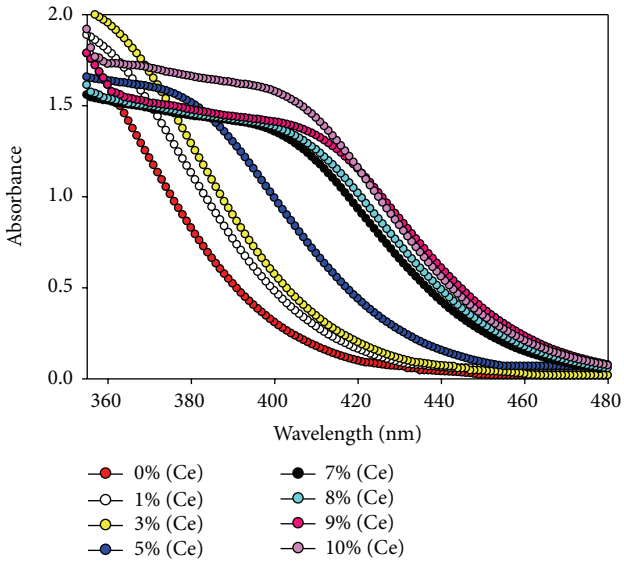

Figure 6: Absorption spectra of undoped and Ce-doped TiO_2.

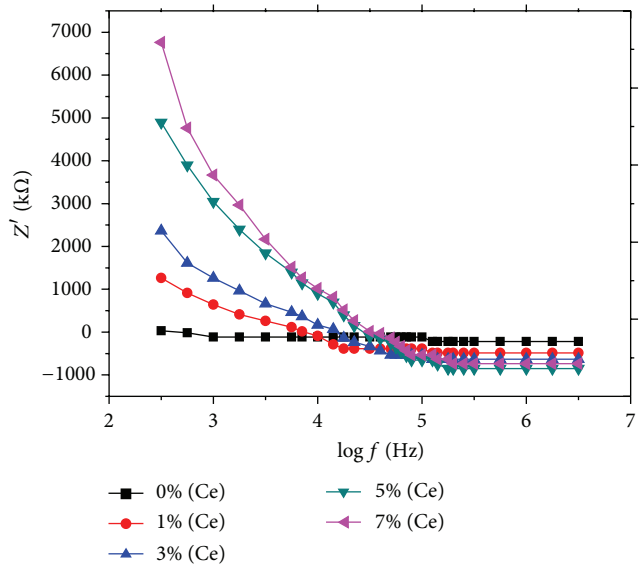

Figure 7: Variation in real impedence Z' as a function of frequency and compositions.

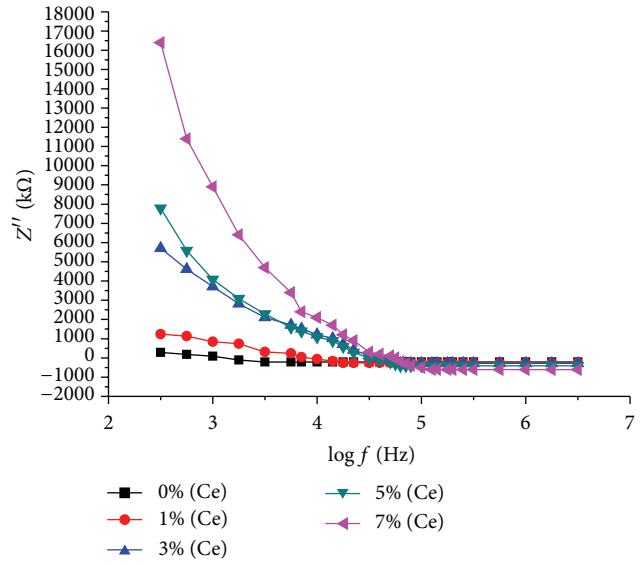

Figure 8: Variation in imaginary impedence Z'' with frequency.

3.2. Electrical Properties

3.2.1. Impedance Analysis. The real part (Z') and imaginary part (Z'') of impedances with frequency at different concentrations of doped TiO_2 are plotted in Figures 7 and 8.

The Z' and Z'' decrease with the increase in frequency because of the space charge polarization [32]. At low frequency the complex impedance values are higher which indicate the larger polarization, whereas at higher frequency the complex impedance shows independent behaviour.

3.2.2. Dielectric Studies. The variation of dielectric constant ($\acute{\varepsilon}$) and tangent loss (tanδ) with frequency for various concentration of doped TiO_2 are plotted in Figures 9 and 10 at room temperature. The dielectric properties of a material depends

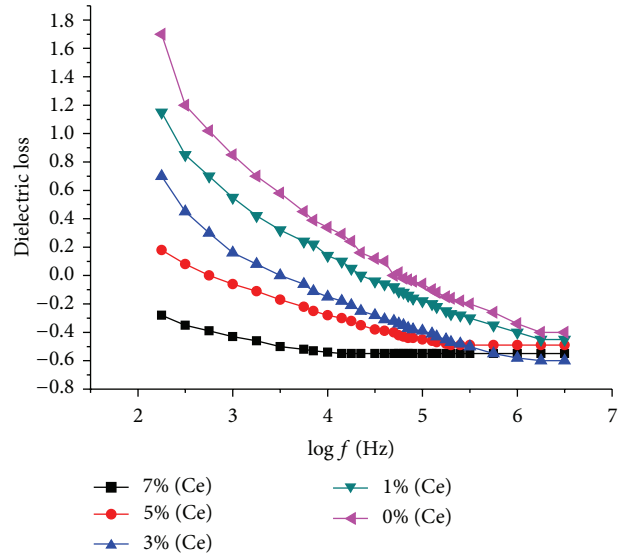

Figure 9: Variation in dielectric loss with frequency at different compositions.

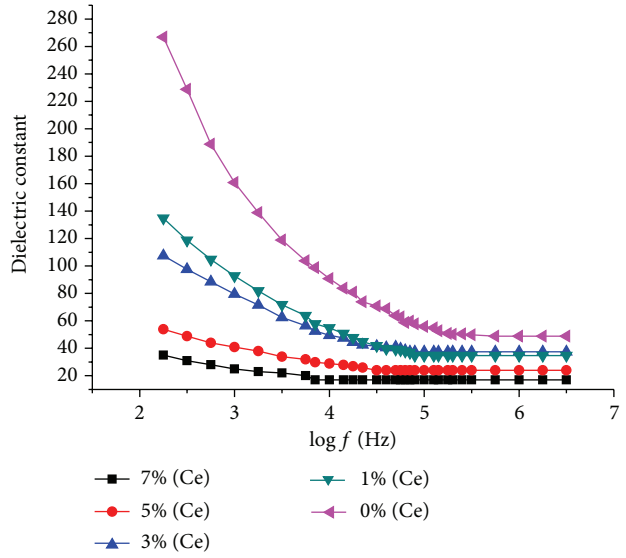

Figure 10: Variation in dielectric constant with frequency for different compositions.

upon different types of polarization, that is, dipolar, electronic, atomic, and space charge polarization.

The values of $\acute{\varepsilon}$ and tan δ decreases with an increase in frequency. At low frequency, the dielectric constant increases due to the accumulation of charge at grain boundary and the sample and electrode interface with each other also called space charge polarization [33]. As the frequency increases the dielectric constant decreases due to the space charge polarization, which diminishes gradually; hence, the electronic and atomic contribution dominates. The dielectric constant is independent at higher frequency indicating the domination of electronic and atomic contribution [16].

3.2.3. a.c. Conductivity. The variation of a.c. conductivity with frequency for different concentration of doped TiO_2 at room temperature are given in Figure 11.

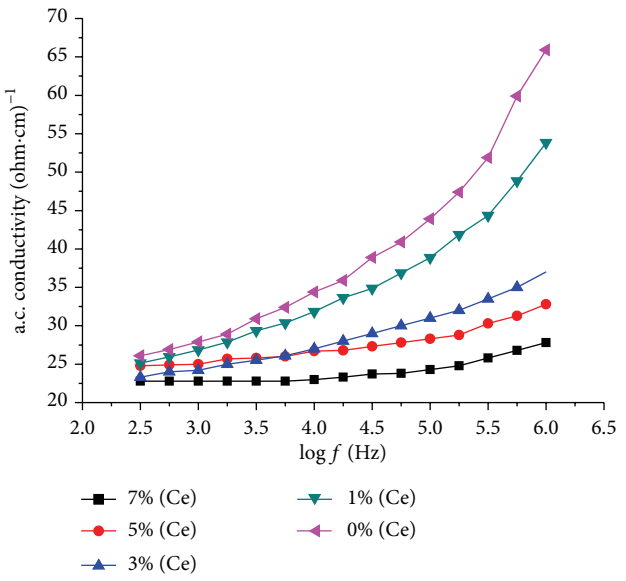

Figure 11: Variation of a.c. conductivity with frequency for different compositions.

The overall conductivity is the sum of a.c. conductivity and d.c. conductivity which is given by

$$\sigma = \sigma_o(T) + \omega\varepsilon_o\varepsilon_r \tan\delta, \quad (3)$$

where ω: angular frequency, ε_o: permittivity of free space, and $\sigma_o(T)$ is the d.c. conductivity and independent of frequency, whereas $\omega\varepsilon_o\varepsilon_r$ tan δ is the a.c. conductivity which is dependent of frequency.

The conductivity increases with the increase in frequency as the electron hopping frequency enhances [15]. It also shows that the a.c. conductivity decreases with the increase in dopant concentration. This may be due to the decrease in the particle size, resulting in increase in the ratio of the surface volume, which indicate the corresponding occurrence of scattering [34].

3.3. Photocatalytic Activity

3.3.1. Effect of Different Percentage of Ce Doping on the Photocatalytic Activity of TiO_2. An aqueous suspension of Remazol Brilliant Blue R (0.05 mM, 200 mL) in the presence of undoped TiO_2 or Ce-TiO_2 (with different concentrations of Ce varying from 1 to 10% calcined at 400°C) was irradiated with 500 W linear visible light halogen lamp at different time interval with constant bubbling of atmospheric oxygen. The degradation of the dye was monitored by measuring the change in absorbance as a function of irradiation time. As a representative example Figure 12 shows the change in absorption intensity of the dye as a function of irradiation time in the presence Ce-doped TiO_2 (9% dopant). Figure 13 shows the change in concentration of the dye as a function of irradiation time in the presence of Ce-doped TiO_2 (1–10%) and absence of Ce-doped TiO_2. It could be seen from the figure that in the presence of undoped TiO_2, very little change in concentration was observed. Whereas in the presence of doped TiO_2 degradation of the dye increases with the increase in dopant

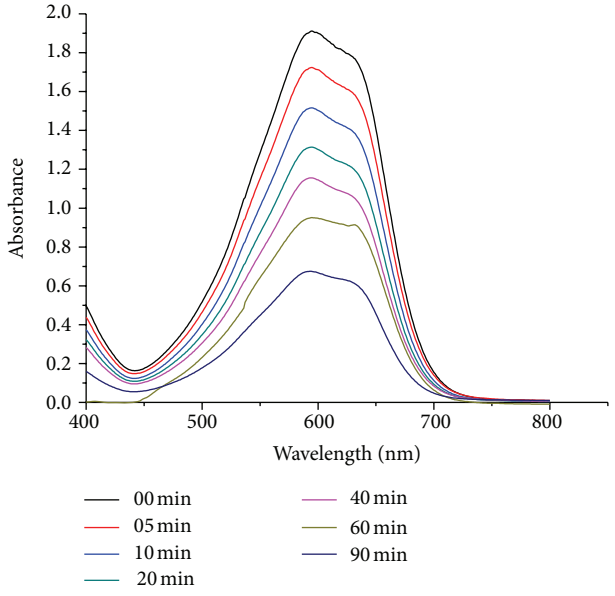

Figure 12: Change in absorbance as a function of time on irradiation of an aqueous solution of Remazol Brilliant Blue R in the presence of Ce-doped TiO_2. *Experimental conditions.* Reaction vessel: immersion well photochemical reactor made up of Pyrex glass, light source: visible light halogen linear lamp (500 W, 9500 Lumens), photocatalyst: Ce-doped TiO_2 (1 g L^{-1}), dopant conc. (Ce) 9% (w/v), Dye (0.05 mM), volume (200 mL), continuous stirring, and air purging. Calcination temperature: 400°C, calcination time: 4 h, and irradiation time: 90 min.

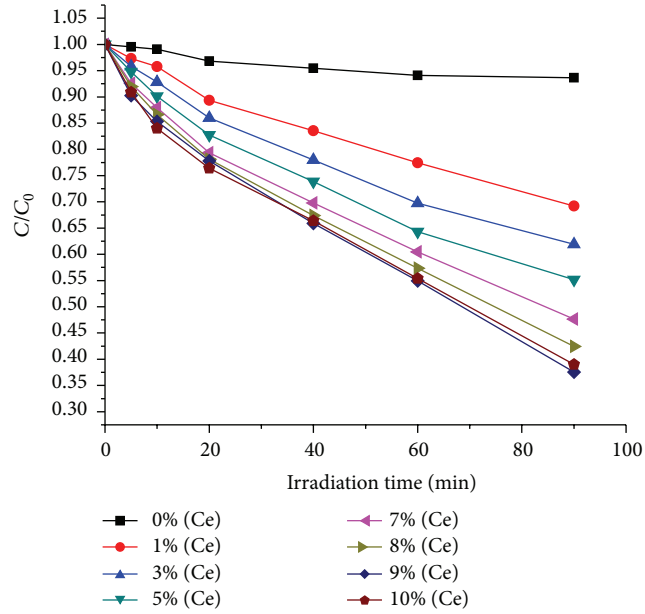

Figure 13: Change in concentration as a function of time on irradiation of an aqueous solution of Remazol Brilliant Blue R in the presence and absence of Ce-doped TiO_2. Experimental conditions. Reaction vessel: immersion well photochemical reactor made up of Pyrex glass, light source: visible light halogen linear lamp (500 W, 9500 Lumens), photocatalyst: Ce-doped TiO_2 (1 gL^{-1}), dopant conc. (Ce) 0, 1, 3, 5, 7, 8, 9, and 10% (w/v), Dye (0.05 mM), volume (200 mL), continuous stirring, and air purging. Calcination temperature: 400°C, calcination time: 4 h, and irradiation time: 90 min.

concentration and the highest degradation was observed with 9% Ce-doped TiO_2 and further increase in the dopant concentration leads to little decrease in the efficiency.

The increase in the photocatalytic activity by increasing the dopant concentration from 1 to 9% may be due to the shortening of band gap thereby effectively absorbing the light of longer wavelength. Another reason for the increase in the photocatalytic activity by increasing the dopant concentration could be attributed to the fact that the doping of TiO_2 with Ce introduces new trapping sites which affects the life time of charge carriers by splitting the arrival time of photogenerated electrons and holes to reach the surface of photocatalyst and thus electron-hole recombination is reduced. At higher dopant concentration (10%) there is occurrence of multiple trapping of charge carriers and hence the possibility of electron-hole recombination increases [35, 36] and fewer charge carriers will reach the surface to initiate the degradation of the dye; hence, decrease in degradation efficiency at higher dopant concentration was observed.

The slow degradation of Remazol Brilliant Blue R in the presence of undoped TiO_2 under visible light irradiation could be due to the direct absorption of light by the dye molecule and can lead to charge injection from the excited state of the dye to the conduction band of the semiconductor as summarized in the following equations:

$$\mathrm{Dye_{ads}} + h\nu \longrightarrow \mathrm{Dye^{*}_{ads}} \quad (4)$$

$$\mathrm{Dye^{*}_{ads}} + \mathrm{TiO_2} \longrightarrow \mathrm{Dye^{+}_{ads}} + \mathrm{TiO_2}\,(\mathrm{e^{-}}) \quad (5)$$

The mechanism of TiO_2 doped with Ce could be visualised as follows. Doping of TiO_2 with Ce introduces a new energy level (Ce impurity level) by the dispersion of metal nanoparticles in the TiO_2 matrix which acts as electron trap [37]. The trap of electron can inhibit electron-hole recombination during irradiation thereby increasing the lifetime of charge carriers. The doping of TiO_2 with Ce not only improves the separating efficiency of photoinduced electrons and holes, but it also increases the visible light absorption due to shortening of band gap. The mechanism of doped TiO_2 can be represented by the following equations:

$$\mathrm{TiO_2} + h\nu \longrightarrow \mathrm{e^{-}_{CB}} + \mathrm{h^{+}_{VB}} \quad (6)$$

$$\mathrm{M} + h\nu \longrightarrow \mathrm{e^{-}} + \mathrm{M^{+}} \quad (7)$$

$$\mathrm{M^{+}} + \mathrm{e^{-}_{VB}} \longrightarrow \mathrm{M} \quad (8)$$

$$\mathrm{O_2} + \mathrm{e^{-}_{CB}} \longrightarrow \mathrm{O_2^{-\bullet}} \quad (9)$$

$$\mathrm{H_2O} + \mathrm{h^{+}_{VB}} \longrightarrow {}^{\bullet}\mathrm{OH} + \mathrm{H^{+}} \quad (10)$$

M corresponds to doped Metal.

On absorption of photon of energy equal to or greater than its band gap by the TiO_2 particle, an electron may be promoted from the valence band to the conduction band (e^{-}_{CB}) leaving behind an electron vacancy or "hole" in the valence band h^{+}_{VB}. Similarly, an electron may be promoted from impurity level to conduction band of TiO_2 by absorbing

photon of energy equaling to or greater than its band gap. The vacancy created in the impurity band acts as electron trap. The electron generated in the valence band of TiO_2 is trapped by the electron trap thereby reducing the electron-hole recombination. If charge separation is maintained, the electron and hole may migrate to the catalyst surface where they participate in redox reactions with sorbed species. Specially, h^+_{VB} may react with surface bound H_2O or OH^- to produce the hydroxyl radical and (e^-_{CB}) is picked up by oxygen to generate superoxide radical anion.

4. Conclusion

The doping of Ce into TiO_2 lattice shifts the position of its fundamental absorption edge towards the longer wavelength and reduces its band gap energy so that it can absorb energy from a major portion of visible light. The XRD analysis shows no change in crystal structure of TiO_2 after doping with different concentration of Ce indicating single-phase polycrystalline material. The SEM and FTIR analysis shows the crystalline nature and anatase phase of undoped and doped TiO_2, respectively. The TEM analysis shows that particles are in the range of 9–14 nm in size. In the low frequency region the dielectric constant decreases with increase in frequency, whereas in the high frequency region it shows the frequency independent behavior, and at high frequency dielectric loss is constant so it can be used for high frequency devices. Ce-TiO_2 also shows that a high dielectric constant and low dielectric loss with frequency imply that the material is suitable for microelectronic device applications. As the frequency increases the magnitude of complex impedance decreases resulting in the increase in a.c. conductivity. It is also observed that the impedance increases with the increase in dopant concentration, resulting in the decrease in a.c. conductivity. The doped TiO_2 was found to be more efficient for the degradation of dye under visible light source as compared to undoped TiO_2.

Conflict of Interests

The authors declare that they do not have any financial relation with the commercial identities or associative interests that represents a conflict of interest in connection with the work submitted.

Acknowledgments

Financial Support by the Council of Science and Technology, U.P. for providing young scientist award under young scientist scheme to Dr. M. M. Haque (Ref no. CST/YSS/D-3916) and UGC New Delhi for granting Maulana Azad National Fellowship for Minority Student to Aisha Malik (no. F.40-3(M/S)/2009(SA-III/MANF)), and the Centre for Excellence in Nano-Technology, Department of Applied Physics and Department of Chemistry, Aligarh Muslim University, Aligarh for providing necessary facilities are gratefully acknowledged.

References

[1] A. Zaleska, "Doped-TiO_2: a review," *Recent Patents on Engineering*, vol. 2, no. 3, pp. 157–164, 2008.

[2] O. Legrini, E. Oliveros, and A. M. Braun, "Photochemical processes for water treatment," *Chemical Reviews*, vol. 93, no. 2, pp. 671–698, 1993.

[3] T. Sugimoto, X. Zhou, and A. Muramatsu, "Synthesis of uniform anatase TiO_2 nanoparticles by gel-sol method: 3. Formation process and size control," *Journal of Colloid and Interface Science*, vol. 259, no. 1, pp. 43–52, 2003.

[4] G. Colón, M. Maicu, M. C. Hidalgo, and J. A. Navío, "Cu-doped TiO_2 systems with improved photocatalytic activity," *Applied Catalysis B*, vol. 67, no. 1-2, pp. 41–51, 2006.

[5] X. Fan, X. Chen, S. Zhu et al., "The structural, physical and photocatalytic properties of the mesoporous Cr-doped TiO_2," *Journal of Molecular Catalysis A*, vol. 284, no. 1-2, pp. 155–160, 2008.

[6] H. Zhang and H. Zhu, "Preparation of Fe-doped TiO_2 nanoparticles immobilized on polyamide fabric," *Applied Surface Science*, vol. 258, pp. 10034–10041, 2012.

[7] B. Liu, X. Wang, G. Cai, L. Wen, Y. Song, and X. Zhao, "Low temperature fabrication of V-doped TiO_2 nanoparticles, structure and photocatalytic studies," *Journal of Hazardous Materials*, vol. 169, no. 1–3, pp. 1112–1118, 2009.

[8] V. D. Binas, K. Sambani, T. Maggos, A. Katsanaki, and G. Kiriakidis, "Synthesis and photocatalytic activity of Mn-doped TiO_2 nanostructured powders under UV and visible light," *Applied Catalysis B*, vol. 113-114, pp. 79–86, 2012.

[9] Y. Tseng and C. Kuo, "Photocatalytic degradation of dye and NOx using visible-light-responsive carbon-containing TiO_2," *Catalysis Today*, vol. 174, no. 1, pp. 114–120, 2011.

[10] U. G. Akpan and B. H. Hameed, "The advancements in sol-gel method of doped-TiO_2 photocatalysts," *Applied Catalysis A*, vol. 375, no. 1, pp. 1–11, 2010.

[11] E. D. Jeong, P. H. Borse, J. S. Jang et al., "Hydrothermal synthesis of Cr and Fe co-doped TiO_2 nanoparticle photocatalyst," *Journal of Ceramic Processing Research*, vol. 9, no. 3, pp. 250–253, 2008.

[12] D. H. Kim, S. I. Woo, S. H. Moon et al., "Effect of Co/Fe co-doping in TiO_2 rutile prepared by solid state reaction," *Solid State Communications*, vol. 136, no. 9-10, pp. 554–558, 2005.

[13] R. Asahi, T. Morikawa, T. Ohwaki, K. Aoki, and Y. Taga, "Visible-light photocatalysis in nitrogen-doped titanium oxides," *Science*, vol. 293, no. 5528, pp. 269–271, 2001.

[14] M. Muruganandham and M. Swaminathan, "Solar photocatalytic degradation of a reactive azo dye in TiO_2-suspension," *Solar Energy Materials and Solar Cells*, vol. 81, no. 4, pp. 439–457, 2004.

[15] A. Azam, A. S. Ahmed, M. Chaman, and A. H. Naqvi, "Investigation of electrical properties of Mn doped tin oxide nanoparticles using impedance spectroscopy," *Journal of Applied Physics*, vol. 108, no. 9, Article ID 094329, 6 pages, 2010.

[16] M. H. Mangrola, B. H. Parmar, A. S. Pillai, and V. S. Joshi, "Structural, optical and electrical properties of titanium dioxide nanoparticle," *Multi Disciplinary Edu Global Quest*, vol. 1, pp. 138–145, 2012.

[17] P. J. Martin, "Ion-based methods for optical thin film deposition," *Journal of Materials Science*, vol. 21, no. 1, pp. 1–25, 1986.

[18] W. D. Brown and W. W. Grannemann, "C-V characteristics of metal-titanium dioxide-silicon capacitors," *Solid State Electronics*, vol. 21, no. 6, pp. 837–846, 1978.

[19] T. Fuyuki and H. Matsunami, "Electronic properties of the interface between Si and TiO_2 deposited at very low temperatures," *Japanese Journal of Applied Physics*, vol. 25, no. 9, pp. 1288–1291, 1986.

[20] D. Mardare and G. I. Rusu, "Comparison of the dielectric properties for doped and undoped TiO_2 thin films," *Journal of Optoelectronics and Advanced Materials*, vol. 6, no. 1, pp. 333–336, 2004.

[21] N. K. Singh, P. Kumar, A. Kumar, and S. Sharma, "Dielectric relaxation, electrical conductivity and impedance response of barium titanate and strontium titanate doped $Ba(Fe_{0.5}Nb_{0.5})O_3$ Ceramics," *Journal of Engineering and Technology*, vol. 4, pp. 104–113, 2012.

[22] A. L. Patterson, "The scherrer formula for X-ray particle size determination," *Physical Review*, vol. 56, no. 10, pp. 978–982, 1939.

[23] Y. Wang, L. Zhang, S. Li, and P. Jena, "Polyol-mediated synthesis of ultrafine TiO_2 nanocrystals and tailored physiochemical properties by Ni doping," *Journal of Physical Chemistry C*, vol. 113, no. 21, pp. 9210–9217, 2009.

[24] Y. Lin, Y. Chang, W. Yang, and B. Tsai, "Synthesis and characterization of ilmenite $NiTiO_3$ and $CoTiO_3$ prepared by a modified Pechini method," *Journal of Non-Crystalline Solids*, vol. 352, no. 8, pp. 789–794, 2006.

[25] D. H. Kim, H. S. Park, S. Kim, and K. S. Lee, "Synthesis of novel TiO_2 by mechanical alloying and heat treatment-derived nanocomposite of TiO_2 and $NiTiO_3$," *Catalysis Letters*, vol. 106, no. 1-2, pp. 29–33, 2006.

[26] B. M. Reddy and I. Ganesh, "Characterization of La_2O_3-TiO_2 and V_2O_5/La_2O_3-TiO_2 catalysts and their activity for synthesis of 2,6-dimethylphenol," *Journal of Molecular Catalysis A*, vol. 169, no. 1-2, pp. 207–223, 2001.

[27] B. M. Reddy, I. Ganesh, E. P. Reddy, A. Fernández, and P. G. Smirniotis, "Surface characterization of Ga_2O_3-TiO_2 and V_2O_5/Ga_2O_3-TiO_2 catalysts," *Journal of Physical Chemistry B*, vol. 105, no. 26, pp. 6227–6235, 2001.

[28] V. Štengl, S. Bakardjieva, and N. Murafa, "Preparation and photocatalytic activity of rare earth doped TiO_2 nanoparticles," *Materials Chemistry and Physics*, vol. 114, no. 1, pp. 217–226, 2009.

[29] V. Štengl and S. Bakardjieva, "Molybdenum-doped anatase and its extraordinary photocatalytic activity in the degradation of Orange II in the UV and vis regions," *Journal of Physical Chemistry C*, vol. 114, no. 45, pp. 19308–19317, 2010.

[30] K. M. Parida and N. Sahu, "Visible light induced photocatalytic activity of rare earth titania nanocomposites," *Journal of Molecular Catalysis A*, vol. 287, no. 1, pp. 151–158, 2008.

[31] L. G. Devi and B. N. Murthy, "Characterization of Mo doped TiO_2 and its enhanced photo catalytic activity under visible light," *Catalysis Letters*, vol. 125, no. 3-4, pp. 320–330, 2008.

[32] B. S. Rao, B. R. Kumar, V. R. Reddy, T. S. Rao, and G. V. Chalapathi, "AC impedence spectroscopy studies on Ni doped Cds nanoparticles prepared by chemical CO-precipitation method," *Chalcogenide Letters*, vol. 9, pp. 517–525, 2012.

[33] A. A. Saif, Z. Ajamal, Z. Sauli, and P. Poopalan, "Frequency dependent electrical properties of ferroelectric $Ba_{0.8}Sr_{0.2}$ TiO_2 thin film," *Materials Science*, vol. 17, pp. 186–190, 2011.

[34] A. K. Abdul Gafoor, J. Thomas, M. M. Musthafa, and P. P. Pradyumnan, "Effects of Sm^{2+} doping on dielectric properties of anatase TiO_2," *Journal of Electronic Materials*, vol. 40, no. 10, pp. 2152–2158, 2011.

[35] J. Liqiang, S. Xiaojun, X. Baifu, W. Baiqi, C. Weimin, and F. Honggang, "The preparation and characterization of la doped TiO_2 nanoparticles and their photocatalytic activity," *Journal of Solid State Chemistry*, vol. 177, no. 10, pp. 3375–3382, 2004.

[36] K. Wilke and H. D. Breuer, "The influence of transition metal doping on the physical and photocatalytic properties of titania," *Journal of Photochemistry and Photobiology A*, vol. 121, no. 1, pp. 49–53, 1999.

[37] M. Ni, M. K. H. Leung, D. Y. C. Leung, and K. Sumathy, "A review and recent developments in photocatalytic water-splitting using TiO_2 for hydrogen production," *Renewable and Sustainable Energy Reviews*, vol. 11, no. 3, pp. 401–425, 2007.